Renewable Energy 125 (2018) 648–654

Contents lists available at ScienceDirect

Renewable Energy

journal homepage: www.elsevier.com/locate/renene

Solar extinction measurement system based on digital cameras. Application to solar tower plants

J. Ballestrín [a, *], R. Monterreal [a], M.E. Carra [a], J. Fernández-Reche [a], J. Polo [b], R. Enrique [a], J. Rodríguez [a], M. Casanova [a], F.J. Barbero [c], J. Alonso-Montesinos [c], G. López [d], J.L. Bosch [d], F.J. Batlles [c], A. Marzo [e]

[a] CIEMAT-Plataforma Solar de Almería, Solar Concentrating Systems Unit, Almería, Spain
[b] Photovoltaic Solar Energy Unit (Renewable Energy Division, CIEMAT), Madrid, Spain
[c] Departamento de Física Aplicada, Universidad de Almería, Spain
[d] Dpto. Ingeniería Eléctrica y Térmica, de Diseño y Proyectos, Universidad de Huelva, Spain
[e] Universidad de Antofagasta, Centro de Desarrollo Energético Antofagasta, Chile

ARTICLE INFO

Article history:
Available online 5 March 2018

Keywords:
Solar extinction measurement on CSP
Solar tower plants
Extinction coefficient
Digital cameras
Lambertian target

ABSTRACT

In Concentrating Solar Power (CSP) technologies, direct solar radiation is reflected from a concentrating system to a receiver, where it is transformed into process heat. In particular, in solar tower plants, the phenomenon of atmospheric extinction between both systems must be studied since the radiative losses can be important due to the increasingly large distances in the gradually larger plants. Large distances are necessary in order to measure the extinction since, in reduced distances, it can be undetectable. However, the great uncertainty of some available instruments and/or the monochromaticity of others, make it possible to affirm that, at present, there is no experimental device that allows a credible measure of solar extinction to be carried out. Nowadays, digital cameras are used in many scientific applications due to their ability to convert available light into digital images. Their broad spectral range, high resolution and high signal to noise ratio, make them an interesting device for extinction measurement. The aim of this work is to present the description of a novel measurement system for solar extinction at ground level based on two digital cameras and a Lambertian target. The first experimental results show that the system can measure solar extinction in the bandwidth 400–1000 nm with an accuracy of less than an absolute ±2%. This measurement system is currently running on a daily basis at Plataforma Solar de Almería.

1. Introduction

Atmospheric extinction of solar radiation reflected by heliostats on a receiver is recognized as an important cause of energy loss in the increasingly larger solar tower plants. This energy loss increases with the content of atmospheric water vapour and aerosols in the heliostat-receiver path due to the absorption and scattering mechanisms. During the design of these plants, it would be desirable extinction maps similar to the solar resource's ones. It would also be beneficial to have real information on extinction during the daily operation of the tower plants. Unfortunately, there is no standardized measurement method for this and currently the plants are designed, built and operated without knowing this local parameter. The marked local character of this phenomenon and its temporal variability makes it unfeasible to extrapolate extinction models to different sites and seasons.

Some authors have measured the extinction with pyrheliometers. Sengupta and Wagner's study [1] provides a model for attenuation losses between heliostat and receiver in a central receiver system that depends only on DNI measurements. This model relies on the fact that, atmospheric constituents that are not well mixed but significantly influence DNI are mainly present close to the surface. In the case of Tahbouba's work [2], four different pyrheliometers have been used at different altitudes. From the analysis of these measurements, a model was designed in order to simulate the attenuation of direct irradiance with distance of propagation.

There exist commercially available and documented instruments

* Corresponding author.
E-mail address: jesus.ballestrin@psa.es (J. Ballestrín).

https://doi.org/10.1016/j.renene.2018.03.004
0960-1481/

that measure visibility, which is related to atmospheric transmission at 550 nm following the Koschmieder approximation [3] and neglecting the spectral variation of the extinction coefficient. However, the extension to the overall solar spectral range is not trustworthy. The inverse proportionality between the visibility and the extinction coefficient is only applicable under very limited conditions which are far away from reality. These instruments are frequently used at airports to estimate the atmospheric visibility, taking measurements at a few meters distance and then extrapolating them to larger distances. Transmissometers quantify visibility by measuring the light extinction of the atmosphere between the transmitter and the receiver, situated at a limited distance from each other. The light source of these instruments is spectrally quite different to the solar distribution and the application path is very different from the real heliostat-receiver slant ranges. Another type of optical instruments, called scatterometer, are based on forward light scattering, placing the transmitter and the receiver less than 1 m apart with their optical axes crossing each other at a certain angle. However, the small sample volume, without taking into account the atmospheric absorption, the monochromaticity and the influence of the sensor body in the phenomenon, makes the results non representative of the extinction of the atmosphere in a larger spatial area. Based on some of these instruments, several measurement methods have been proposed in recent years but without giving a sufficiently sound solution to the problem to be considered reliable for the measurement of solar energy extinction [4,5]. Nowadays, digital cameras are used in many scientific applications due to their ability to convert available light into digital images. Their broad spectral range, high resolution and high signal to noise ratio, make them an interesting device in solar technology [6]. In a previous work regarding air pollution research, Du et al. [7] developed a digital optical method to measure atmospheric visibility. In Du's method, two digital images of the same target were taken at two different distances in the same straight line. The images were analyzed to determine the optical contrast between the target and its sky background, and visibility was calculated. In previous works, we have shown the order of magnitude of the extinction with the distance in certain scenarios [8], which gave the necessary resolution to measure this parameter correctly. We have also conceptually shown previously the methodology to measure atmospheric extinction using two digital cameras and a Lambertian target [9]. This work describes this measurement system in detail, showing the configuration and instrumentation that is being used at Plataforma Solar de Almería (PSA) and the accuracy in extinction measures. An analysis of the first extinction measurements is presented.

2. Experimental setup for solar extinction measurement

The aim of this measurement system is to take simultaneous images of the same target at very different distances using two identical optical systems with digital cameras, suitable lenses and filters. A topographic study shows a distance between cameras of 741.63 ± 0.01 [10] meters which, in view of previous simulation studies, is considered sufficient to detect the phenomenon and to carry out the measurement [8]. The distances of the cameras to the centre of the target have been chosen (82.88 ± 0.01 m, 824.51 ± 0.01 m) [10]so that the target area projected per pixel is similar in both cameras, 10.4 mm in diameter for the nearest camera and 11.2 mm for the farthest camera. In this procedure, it is necessary to work with diffuse solar radiation reflected by the target in order to avoid direct solar radiation and thus, minimize specular influences and directionality. For this reason, the target and the two cameras were placed in a north-south line; the target was situated south looking north, to avoid the direct solar radiation and the cameras were located north pointing towards the target. The intensity levels of the digital images were proportional to the diffuse solar radiance coming from the target and the difference of intensity between the images was due to the extinction of the solar radiation in the path between both cameras.

Radiance is a measure of the flux density per unit solid viewing angle and it is independent of the distance to an extended area source because the sampled area increases with distance, cancelling inverse square losses [11–13]. The law of conservation of radiance allows us to affirm that the losses of detectable energy between target and cameras are due to the atmospheric extinction in the spectral range of the cameras. The refractive effects of light at these distances are considered negligible.

2.1. Digital cameras, lenses and ND filters

A CCD or CMOS sensor, proportionally transforms the incoming luminous energy from each point of a scene into an electrical signal. Such sensor is composed of photo-sensitive cells called pixels. It is an element in the acquisition chain, located, on one hand, behind an optical system which focuses the image on the photosensitive cells and, on the other hand, in front of an electronic system which amplifies the output signal for digitization. All these elements can produce errors in the measurements. They are called *systematic errors* or *systematic noise*, meaning that they are repeatable. Knowing the patterns of these errors allows us to develop some methods to eliminate the noise in the images. Whatever the application is, the pre-processing that allows the extraction of the useful information from the image inside the noisy signal, is required [14,15]. Several digital cameras (CCD and CMOS) have been tested in the Radiometry Laboratory at PSA using an Ulbricht sphere (integrated sphere) as homogeneous halogen light source. Using neutral density filters and different exposure times, we were able to detect different homogeneous luminance levels with the digital cameras. The chosen camera to measure solar atmospheric extinction has the following interesting properties:

1. High signal to noise ratio: Images from the homogeneous light supplied by an Ulbricht sphere have been taken with the camera. Considering the ratio between the standard deviation and the mean value (σ/μ) from images as figure of merit, the values obtained were under 1%.
2. High resolution (16 bits): Using a neutral density filter and different exposure times, it was possible to detect intensity levels as close as 1.5%, which was enough resolution to detect the expected extinction levels.
3. *Spectral range 400-1000 nm*: About a 73% of the extinction occurs in the spectral range of the camera, which is quite representative of total extinction [9]. Future digital cameras could be based on graphene-CMOS integration which would be sensitive to UV, visible and infrared light (300–2000 nm) [16]. Approximately 98% of the solar extinction phenomenon would take place in this promising bandwidth.

Two sensors are widely used in digital photography: charged couple device (CCD) and complimentary metal-oxide semiconductor (CMOS). Traditionally, due to their superior image quality, CCD cameras were used for scientific purposes, which is why flux measurements have been conducted with CCD cameras [6]. With modern technology however, CMOS sensors have reached image parity with CCD. Furthermore, CMOS offers more chip functionality, lower power dissipation, smaller system size and lower price and are therefore favoured in newer cameras. In a CMOS chip, each pixel has its own charge-voltage conversion and the sensor often includes other circuitries, such as noise-correction and amplifiers. The chosen cameras in order to measure solar

atmospheric extinction are two Hamamatsu® cameras, model ORCA-flash4.0 v3 CMOS, A/D conversion 16 bits output, effective number of pixels 2048(H) x 2048(V), cell size 6.5 μm × 6.5 μm, quantum efficiency higher than 82% at 600 nm and 60% at 750 nm, exposure time 1 m s to 10 s.

The two chosen lenses are Sigma®, model APO 50–500 mm F4.5–6.3 DG OS HSM (Zoom range: 50–500 mm). Working with these different focal distances, it is possible to obtain the same area of target image on pixel in both cameras despite having a great distance between them.

Neutral density filters are attached to the lenses to prevent light over-saturation. These filters are designed to reduce light intensity over a specific wavelength range without affecting the image's contrast. The chosen filters are MIDOPT® (Midwest Optical Systems), flat response range [400–2000] nm, 6.25% transmittance.

Cameras, lenses and filters were installed in refrigerated containers to minimize the influence of thermal noise in the images and to preserve the cameras of the external environment. A heat resistance was installed in each container to prevent internal condensation. Borosilicate windows of high transmittance allow taking images from the interior of the containers through them. The cleaning of the optical systems occurred every day before the image acquisition process. The chosen software for image acquisition and processing was ImagePro Plus, 7.0 (Media Cybernetics®). The cameras were operated by laptops connected to the network to allow a remote use (Fig. 1).

As in all real systems, the hardware used to capture the image has some limitations. These limitations cause imperfections which manifest themselves as image imperfections or noise. Noise is any additive, unwanted measurement that is generated by the sensor independently of incoming light. There are two types: random noise and systematic noise. Random noise cannot be predicted and varies from one image to another. Systematic noise, on the other hand, can be predicted and compensated for, if necessary. The major sources of systematic noise that can be compensated for are: bias, vignetting and imperfect sensors [14,15].

Fig. 1. Camera, lens and laptop in a container.

2.1.1. Bias

Taking a dark frame image (an image generated in the absence of any incoming light), each pixel should read zero since no light is falling on the pixel. However, zero values in a dark frame are purposefully avoided in camera design as any value below zero will also be read as zero. Therefore, to account the uncertainty, digital camera manufacturers deliberately insert an offset value above zero. In order to account for bias, a dark frame or bias frame should be removed from all experimental images.

A set of dark images was taken with each camera for 3 h, in total 36 images, one every 5 min. A similar behavior was observed in both and the results were consistent with the manufacturer's specifications. In particular, the statistic of the dark average image for Camera 1 (average1 = 98.9, stdv1 = 1.1, deviation 1 = 1.1%) and for Camera 2 (average2 = 99.4, stdv2 = 1.7, deviation2 = 1.7%) represented 1–2 intensity levels, uncertainty that can be neglected when working at 80–90% of cameras dynamical range ($2^{16}-1 = 65535$), as we were. As a consequence of this analysis and, since our measurement procedure is a differential process, we decided not to subtract the dark image from our images to avoid introducing unnecessary uncertainties. The stability of both cameras will be checked periodically by a similar test.

2.1.2. Bias vignetting or shading

Vignetting is an imaging phenomenon that happens with every optical system. It is a radially dependent illumination strength falloff due to the camera lens and optical properties of the system. All lens systems have light ray spread which increases as the light rays are further from the center. Vignetting results in a radial shadowing effect towards the image periphery [14,15].

The image is brighter in the center than the edges. The importance of this effect depends on the optical configuration that is used (long or short focal length and large or small aperture) and the measurement process to be carried out.

2.1.3. Imperfect sensors

The third influence of noise is due to the fact that the sensor pixels are not perfectly manufactured. This imperfect manufacturing shows up as per-pixel noise. In order to correct for both vignetting and errors associated with imperfect pixel sensors, a flat field image is captured. Flat fields are fields which exhibit even illumination. Flat field images were generated by an Ulbricht sphere, which is considered the best way to obtain them. Exposure time is set long enough to be close to the saturation of the sensor in order to ensure that a significant signal level is recorded. Flat field images under the effects of vignetting exhibit radial deviation away from a uniform condition. Several flat field images should be captured and the mean correction factor determined. The correction of the raw image should be done by a pixel-wise division with the flat field image. Then, the obtained image should be multiplied by a coefficient equal to the mean value of flat field image. This keeps some levels close to the ones in the original image. The treatments should be done on pre-processed images with offsets image correction which is subtracted only one time [14,15]. In our case, as we worked with great distances and paraxial optics, the target images represent a small percentage of the central part of the field of view of the lenses, which made the shading effect quantitatively negligible in our measurement process. As a result of this

analysis, we decided not to perform shading correction on our images in order to avoid unnecessary manipulations of what we want to measure.

In spite of having two identical optical systems, it was necessary to determine the minimum intrinsic offset between them both and take it into account when treating the images. For this, we chose the most optimal conditions of reference in a moment and day of high DNI and minimum extinction according to magnitudes and relevant parameters in the phenomena of atmospheric extinction, which are relative humidity (RH), particle concentration, Aerosol Optical Thickness (AOT, i.e. the vertical integral of the extinction coefficient along the atmosphere) at different wavelengths (http://aeronet.gsfc.nasa.gov/), atmospheric pressure and wind speed. The exposure times chosen that day for each camera (9 ms and 15 ms) guaranteed a high level of luminous intensity without reaching the saturation in the images throughout the year and a constant offset between cameras. However, occasionally some images have saturation due to unexpected solar reflections by clouds on the target. In these cases, the extinction measure is rejected. The appearance of better conditions would be detected by the system and would allow correcting previous measures taking into account the new offset.

2.2. Lambertian target

Having Lambertian targets is important for this measurement system since the position of the cameras and the angles relative to the target can never be known for sure at such large distances. With a perfect diffuser surface, an image of the target taken from any viewing angle will accurately represent the same brightness or luminance. For this setup a target of appreciable dimensions (2 m × 2 m) was needed and its specific manufacturing was necessary. The target was supported on two pillars, approximately 1 m above the ground. It had two side doors that remained closed when it was not used in order to protect it from rain, dust, etc. Two standard steel plates of 2 m × 1 m were used for their construction (Fig. 2). Both were sandblasted to achieve diffusivity on their surface. Unfortunately this treatment was not enough and it was necessary to apply a special coating for this purpose. A number of different paints were tested and it was found that white Amercoat®741 and black Zynolyte® had suitable diffuser properties. For this study, one of the steel plates was painted in high reflectance white and the other was sprayed in black (Fig. 2).

The white part of the target had a weighted solar reflectance of 76% after being painted. The black part of the target had a weighted solar absorptance of 95% [17] and the image taken from this part was considered as the airlight contribution or light scattered in the air by dust, haze, etc. This light contribution, I_B, was suppressed from the light input of the images taken of the white part of the target I_W (Fig. 2). The target was characterized and its good homogeneity and diffusivity were verified [18,19], and was considered suitable for the measurement of solar extinction. The analysis of target images taken with a conventional digital camera showed a dispersion of luminous intensity of 0.3% on the part painted with white Amercoat®741 and 0.2% on the part painted with black Zynolyte® which was proof of adequate homogeneity. Angular tests with a luminancimeter showed that luminance deviations from central value were less than 1% in the central positions ±10°, which confirmed an optimal diffusivity to carry out extinction measures with our system.

3. Extinction measurement

The aim was to take simultaneous images of the same target at different distances using two identical cameras with suitable lenses

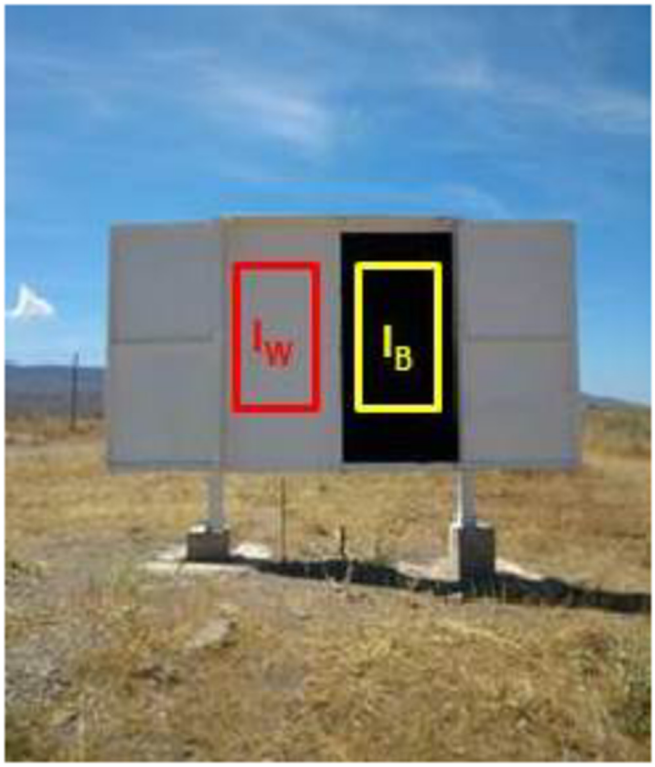

Fig. 2. White and black Lambertian target for extinction measurement. Black (I_B) and white (I_W) zones of interest.

(Fig. 3). In order to do this, we would need to work with diffuse solar radiation projected from the target to avoid direct solar radiation and therefore minimize specular influences and directionality. The intensity levels of the digital images would be proportional to the diffuse radiance coming from the target.

The spatial calibration of both cameras allowed us to select the same areas of the target in the same zones. The areas were selected in the central part of the target to avoid edge effects. These areas were 0.5 × 1 m, same in the white part as in the black part of the target (Fig. 4). They represented 4656 pixels in camera1 and 3961 pixels in camera2, equally in the white zone as in the black zone of the target, which were adequate matrix dimensions to deal with statistically. The intensity difference or light extinction between both images taken was related to the distance between the two cameras and the extinction for the experimental distance (D = 741.63 ± 0.01 m [10]) can be obtained in a direct way by:

$$\textbf{Extinction}(\%) = 100\left(1 - \frac{\mathbf{I_2}}{\mathbf{I_1}}\right) \quad (1)$$

Where I_1 (I_1=I_{1W}-I_{1B}) and I_2 (I_2=I_{2W}-I_{2B}) are the average intensities of the images (Fig. 4) and D (741.63 ± 0.01 m) the distance between the cameras (Fig. 3).

The extinction coefficient (β_{Ext}) can be derived from the Beer-Lambert-Bouguer law by:

Fig. 3. Lambertian target and cameras layout.

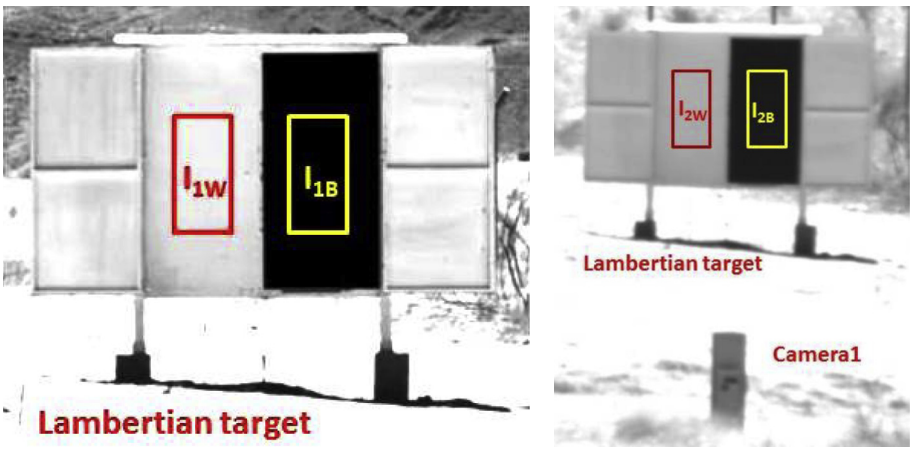

(a) (b)

Fig. 4. Images taken simultaneously with both cameras 03-July-2017 14:00:45 p.m. (a) Camera1. (b) Camera2.

$$\beta_{Ext} = -\frac{\ln \frac{I_2}{I_1}}{D} \quad (2)$$

The uncertainties associated with the measurement of the extinction and extinction coefficient by this procedure are given by:

$$\sigma_{Extinction}(\%) = \pm\frac{100}{I_1}\sqrt{\left(\frac{I_2}{I_1}\right)^2 \sigma_{I_1}^2 + \sigma_{I_2}^2} \quad (3)$$

$$\sigma_{\beta_{Ext}} = \pm\frac{1}{D}\sqrt{\left(\frac{\sigma_{I_1}}{I_1}\right)^2 + \left(\frac{\sigma_{I_2}}{I_2}\right)^2 + \left(\frac{\sigma_D}{D}\right)^2 \left(ln\frac{I_2}{I_1}\right)^2} \quad (4)$$

Where σ_{I1} and σ_{I2} are the standard deviations associated to I_1 and I_2 that are due to camera noise and some lack of homogeneity on the surface of the target. To minimize this random noise, 20 images were taken in less than 1 s in each measurement and the average image of them was considered as the final image [15]. Working outdoors makes it necessary to resort to this smoothing procedure; however, the good performance of the cameras, makes it technically possible. σ_D (0.01 m) represents the uncertainty associated to the distance between the cameras [10].

Previous equations and information obtained from target images taken simultaneously with both cameras, allowed us to obtain uncertainties in the extinction measurements less than absolute ±2%. After several weeks of measurements, most of the extinction values obtained were less than 7%. Such low values of extinction lead to low extinction coefficients with high uncertainties. A campaign of solar extinction measures is under way at PSA to obtain a representative year. In parallel, meteorological variables such as DNI, relative humidity, particle concentration, Aerosol Optical Thickness (AOT, http://aeronet.gsfc.nasa.gov/), atmospheric pressure and wind speed were recorded.

This extinction coefficient could be used in the nearby surroundings to obtain extinction using the same law and the slant range, S_i, of each heliostat i (i = 1, ….n, n = number of heliostats):

$$\mathbf{Extinction_i}(\%) = 100\left(1 - \mathbf{e}^{-\beta_{Ext}\ S_i}\right) \quad (5)$$

The uncertainty associated with the extinction will then be given by:

$$\sigma_{\mathbf{Extinction_i}}(\%) = 100\mathbf{e}^{-\beta_{Ext}\ S_i}\sqrt{\left(\mathbf{S_i}\sigma_{\beta_{Ext}}\right)^2 + \left(\beta_{\mathbf{Ext}}\ \sigma_{S_i}\right)^2} \quad (6)$$

The uncertainty obtained in this way would be slightly higher than that obtained by directly measuring extinction and applying equations (3) and (4).

Applying this methodology during different periods of time will allow us to obtain average extinction coefficients and solar atmospheric extinction models at the selected sites using the form of equation (5) without having to use any simulation tool. In general, the majority of the extinction models in the past [8,20–26] were obtained through elaborated simulation procedures, using radiative transfer codes (MODTRAN, LibRadtran, SMARTS, …) [27–29] and were represented by polynomial expressions that could be adjusted to equation (5) in order to obtain the corresponding extinction coefficient or vice versa. System Advisor Model (SAM), developed by NREL (National Renewable Energy Lab), is a model that allows to calculate the annual electricity production of solar thermal and photovoltaic plants that has proved high reliability for modeling CSP plants [30–32]. The input that describes the technical characteristics of a solar tower plant in SAM requires a third order polynomial coefficients for modeling the solar extinction taking place in the heliostat field. Therefore, the models obtained with our measurement system can be used to predict the annual losses in electricity production in a tower solar plant due to extinction in a selected location.

As mentioned above, the main field of application of this study is in solar tower plants both for the design process and for the daily operation of the plant. In other systems of solar concentration the distances are much more reduced and the influence of the extinction phenomenon can be considered negligible.

4. Extinction measurement results

After the measurement system was put into operation, extinction was measured daily with a 15-min time interval which was considered adequate due to the low variability observed. During July 2017, 184 measures of extinction were obtained simultaneously with RH, AOT (500 nm) and particle concentration (0.25–32 μm, particles/l). A haze episode took place on July 14 and was revealed in the recorded measurements (Fig. 5).

Fig. 5 shows a clear dependence of extinction and extinction coefficient with RH and particle concentration, but not with AOT.

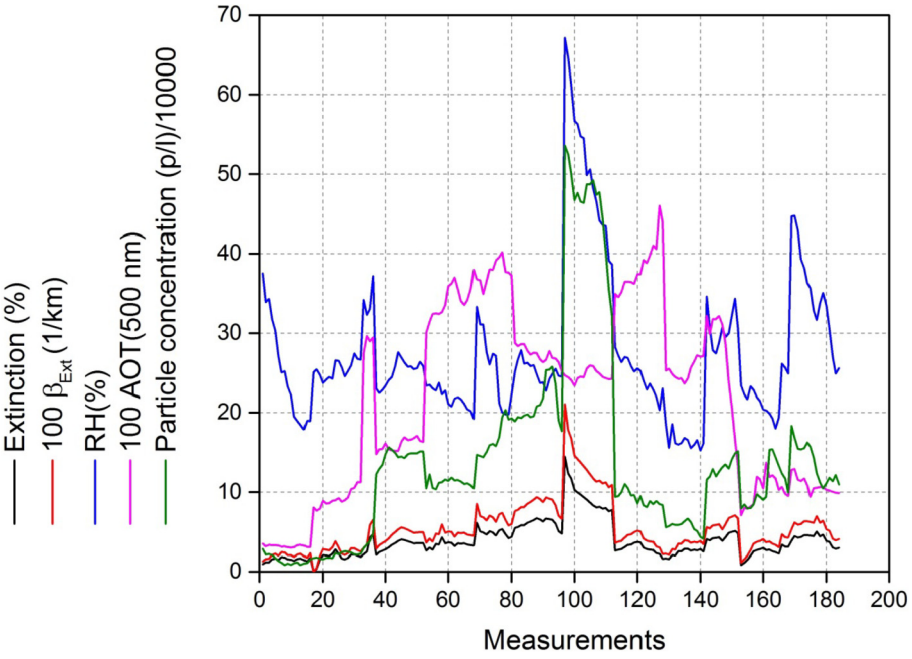

Fig. 5. Extinction(%), 100β_{Ext}(1/km), RH(%), 100AOT (500 nm) and particle concentracion(p/l)/10000 during July 2017. Haze episode on July 14.

The non-dependence of extinction and extinction coefficient with the parameter AOT was observed in other wavelengths (1640, 1020, 870, 675, 440, 380 and 340 nm).

In view of the observed dependencies, we proposed a linear relation of extinction and extinction coefficient with RH and particle concentration (Fig. 6).

$$\textbf{Extinction}(\%) = \boldsymbol{C}_1\ \mathrm{RH}(\%) + \boldsymbol{C}_2\boldsymbol{Particle\ concentration}(\boldsymbol{p}/\boldsymbol{l})/10000 \quad (7)$$

$$\beta_{\boldsymbol{Ext}}(1/\mathbf{km}) = \boldsymbol{C}_3\boldsymbol{RH}(\%) + \boldsymbol{C}_4\boldsymbol{Particle\ concentration}\left(\boldsymbol{p}/\boldsymbol{l}\right)/10000 \quad (8)$$

The values of the constants C1 and C2 are respectively 0.0350 and 0.1724 (l/p). Although the statistics are not very large (N = 184), the results of the canonical correlation analysis performed on the variables showed an important influence on the extinction.

The Normalized Mean Bias Deviation (NMDB) is −3.8% which is interpreted as that the model provides slightly lower extinction values than those measured, probably because more variables influence the phenomena of extinction or that it has not taken into account particles of greater or smaller size. The Normalized Root Mean Square Deviation (NRMSD) is 6.9%. Such a small value indicates low residual variance. Both MDB and RMSD were normalized to the range of the measured extinction ($Extinction_{max}$-$Extinction_{min}$). The Pearson correlation coefficient, R, is 0.9334 meaning an admissible increasing linear relationship. In the case of the extinction coefficient, the values of the constants C3 and C4 were respectively 0.0005 and 0.0025 (l/p), and the relevant statistical parameters were NMBD = −2.3%, MRMSD = 6.1% and R = 0.9348. Although the result was hopeful, more measures must be performed to statistically corroborate this dependence. We must consider that these measures were carried out in summer, which is a period in which the haze processes are common and the extinction is higher.

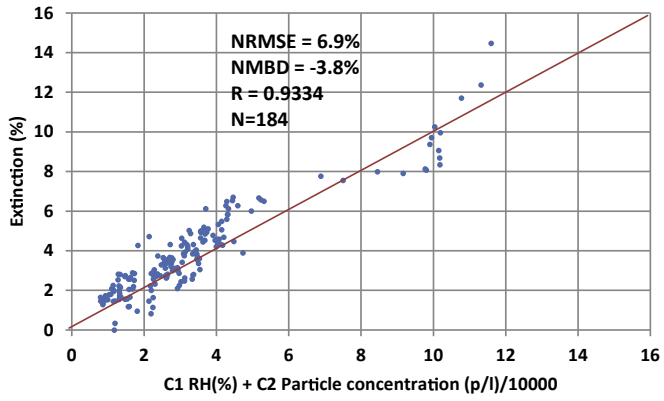

Fig. 6. Measured extinction (%) versus RH (%) and particle concentration (p/l)/10000.

5. Conclusions and outlook

Atmospheric extinction of solar radiation reflected by heliostats to receiver is recognized as an important cause of energy loss in the increasingly large solar tower plants. During the design of these plants, it would be desirable extinction maps similar to the solar resource ones. Unfortunately, the truth is that there is currently no reliable measurement method for solar extinction and, at present, these plants are designed, built and operated without knowing this local parameter.

Nowadays digital cameras are used in many scientific applications for their ability to convert available light into digital images. Their broad spectral range, high resolution and high signal to noise ratio, make them an interesting device in solar technology. In this work, a novel system for solar extinction measurement based on digital images and Lambertian target has been presented. The first experimental results show that the system can measure solar extinction in the bandwidth 400–1000 nm with an accuracy of less than absolute ±2%. The future development of better digital cameras will allow a more accurate extinction measurement and in a

wider spectral range.

This measurement system is currently running daily at PSA in order to obtain a characteristic extinction year. The application of this methodology for periods of time will allow to obtain representative models of solar atmospheric extinction at the chosen sites without having to use simulation tools. The models obtained with our measurement system can be used to predict the annual losses in electricity production in a tower solar plant due to extinction in a certain location.

The analysis of the first measurements has shown a linear relation of extinction and extinction coefficient with relative humidity and particle concentration, but more measures must be performed to statistically corroborate this dependence.

The solar extinction measurement system described in this work could serve as a reference system in intercomparison campaigns with monochromatic measurement instruments such as transmissometers and scatterometers.

Acknowledgements

Financial support by the Ministry of Economy, Industry and Competitiveness under PRESOL project “Forecast of solar radiation at the receiver of a solar power tower”, ENE2014-59454-C3-3-R with ERDF funds. Financial support provided by the Education Ministry of Chile Grant PMI ANT 1656 and 1201 and CONICYT/FONDAP/15110019 "Solar Energy Research Center" SERC-Chile as well. The authors acknowledge the generous financial support provided by the Innova Chile - CORFO, PROJECT CODE: 17BPE3-83761. The authors wish to thank to the principal investigators and staff from AERONET program, and particularly Stefan Wilbert (DLR) directly involved in the station of Tabernas-PSA, for delivering so useful data to the scientific community. Grateful to Natalie Hanrieder (DLR) for providing us the particle concentration data recorded at PSA during the campaign of measures of solar extinction. Thanks to the PSA's Maintenance, Operation, Instrumentation and Informatics staff for the excellent work during the installation and start-up of the system.

References

[1] M. Sengupta, M. Wagner, Atmospheric attenuation in central receiver systems from DNI measurements, in: SolarPACES2012 International Symposium, 2012.
[2] Z. Tahbouba, et al., Modeling of irradiance attenuation from a heliostat to the receiver of a solar central tower, in: SolarPaces2013 International Symposium, 2013.
[3] H. Horvath, On the applicability of the Koschmieder visibility formula, Atmos. Environ. Pergamon 5 (1971) 177–184.
[4] N. Hanrieder, et al., Determination of beam attenuation in tower plants, in: SolarPaces2012 International Symposium, 2012.
[5] N. Hanrieder, et al., Atmospheric extinction in solar tower plants: absorption and broadband correction for MOR measurements, Atmos. Meas. Tech. 8 (2015) 3467–3480.
[6] J. Ballestrín, R. Monterreal, Hybrid heat flux measurement system for solar central receiver Evaluation, Energy 29 (2004) 915–924.
[7] K. Du, et al., Quantification of atmospheric visibility with dual digital cameras during daytime and night time, Atmos. Meas. Tech. 6 (2013) 2121–2130.
[8] J. Ballestrín, A. Marzo, Solar radiation attenuation in solar tower plants, Sol. Energy 86 (2012) 388–392.
[9] J. Ballestrín, et al., Measurement of solar extinction in tower plants with digital cameras, Am. Inst. Phys. Conf. Proc. (2016), https://doi.org/10.1063/1.494921221, 1734, 130002–1–130002-8.
[10] M.A. Montero, Levantamiento topográfico para verificación de distancias en la Plataforma Solar de Almería, Ing. Agrónomo (2017) (Colegiado Nº 2753).
[11] B. Jähne, et al., Handbook of Computer Vision and Applications, Academic Press, 1999.
[12] W. Ross, Introduction to Radiometry and Photometry, Artech House Inc, 1994.
[13] A. Ryer, Light Measurement Handbook, International Light Inc, 1998.
[14] J. Kelcey, A. Lucieer, Sensor correction of a 6-Band multispectral imaging sensor for UAV remote sensing, Remote Sens. 4 (2012) 1462–1493, https://doi.org/10.3390/rs4051462.
[15] A. Mansouri, et al., Development of a protocol for CCD calibration: application to a multispectral imaging system, Int. J. Robotics Automation 20 (2) (2005) 94–100.
[16] S. Goossens, et al., Broadband image sensor array based on graphene-CMOS integration, Nat. Photonics 11 (2017) 366–371.
[17] J. Ballestrín, et al., Calibration of high-heat-flux sensors in a solar furnace, Metrologia Inst. Phys. 43 (2006) 495–500.
[18] J. Ballestrín, et al., Characterization of a lambertian target for measurement techniques on solar concentration, in: SolarPaces2017 International Symposium, 2017.
[19] J. Ballestrín, et al., Diagnosis of a lambertian target in solar context, Measurement 119 (2018) 265–269. https://doi.org/10.1016/j.measurement.2018.01.046.
[20] C.N. Vittitoe, F. Biggs, Terrestrial Propagation Loss, Presented Amer. Sec. ISES meeting, Denver, 1978. August 1978. Sandia release SAND78–1137C.
[21] H.C. Hottel, A simple model for estimating the transmittance of direct solar radiation through clear atmospheres, Sol. Energy 18 (1976) 129–134.
[22] C.L. Pitman, L. Vant-Hull, Atmospheric transmittance model for a solar beam propagating between a heliostat and a receiver, ASES Prog. Sol. Energy (1982) 1247–1251.
[23] B.L. Kistler, A User's Manual for DELSOL3: a Computer Code for Calculating the Optical Performance and Optimal System Design for Solar Thermal Central Receiver Plants, 1986, p. 78. Sandia Laboratories Report, SAND86-8018.
[24] P.L. Leary, J.D. Hankins, A User's Guide for MIRVAL— a Computer Code for Comparing Designs of Heliostat-receiver Optics for Central Receiver Solar Power Plants, 1979, p. 14. Sandia Laboratories Report, SAND77-8280.
[25] J. Polo, et al., Sensitivity study for modelling atmospheric attenuation of solar radiation with radiative transfer models and the impact in solar tower plant production, Sol. Energy 134 (2016) 219–227.
[26] E. Carra, et al., Atmospheric extinction levels of solar radiation at Plataforma Solar de Almería. Application to solar thermal electric plants, Energy 145 (2018) 400–407.
[27] G.P. Anderson, et al., Reviewing atmospheric radiative transfer modeling: new developments in high and moderate resolution FASCODE/FASE and MODTRAN, in: Optical Spectroscopic Techniques and Instrumentation for Atmospheric and Space Research, vol. II, Society of Photo-Optical Instrumentation Engineers, 1996.
[28] B. Mayer, A. Kylling, Technical note: the libRadtran software package for radiative transfer calculations: description and examples of use, Atmos. Chem. Phys. Discuss. 5 (2005) 1319–1381, https://doi.org/10.5194/acpd-5-1319-2005.
[29] C. Gueymard, A simple model of the atmospheric radiative transfer of Sunshine : algorithms and performance assessment, Fla. Sol. Energy Cent. (1995).
[30] A. Dobos, T. Neises, M. Wagner, Advances in CSP simulation technology in the system advisor model, Energy Procedia 49 (2014) 2482–2489, https://doi.org/10.1016/j.egypro.2014.03.263.
[31] M.J. Wagner, Simulation and Predictive Performance Modeling of Utility-scale Central Receiver System Power Plants, 2008.
[32] M.J. Wagner, P. Gilman, Technical Manual for the SAM Physical Trough Model, Contract, 2011. NREL Report No. NREL/TP-5500–51825.